EXPERIMENTAL EXAMINATION OF WIRE MESH DAMPERS SUBJECTED TO LARGE AMPLITUDE DISPLACEMENTS

A Thesis

by

ADAM MATTHEW JONES

Submitted to the Office of Graduate Studies of
Texas A&M University
in partial fulfillment of the requirements for the degree of

MASTER OF SCIENCE

August 2007

Major Subject: Mechanical Engineering

EXPERIMENTAL EXAMINATION OF WIRE MESH DAMPERS SUBJECTED TO LARGE AMPLITUDE DISPLACEMENTS

A Thesis

by

ADAM MATTHEW JONES

Submitted to the Office of Graduate Studies of
Texas A&M University
in partial fulfillment of the requirements for the degree of

MASTER OF SCIENCE

Approved by:

Chair of Committee,	John M. Vance
Committee Members,	Alan Palazzolo
	César Malavé
Head of Department,	Sai Lau

August 2007

Major Subject: Mechanical Engineering

ABSTRACT

Experimental Examination of Wire Mesh Dampers
Subjected to Large Amplitude Displacements. (August 2007)
Adam Matthew Jones, B.S., Texas A&M University
Chair of Advisory Committee: Dr. John M. Vance

Wire mesh dampers are under investigation because they are seen as replacements for squeeze film dampers as a source of direct stiffness and damping at bearing locations. There are several advantages of wire mesh dampers over squeeze film dampers, including: temperature insensitivity, oil-free operation, and the ability to contain large amplitude vibrations. Furthermore, due to their direct damping and lack of cross-coupled stiffness, the wire mesh reduces the response to imbalance and increases the stability of the system. The objective of this research was to determine the properties of wire mesh dampers under large amplitude vibrations. Impact testing was first conducted on the wire mesh as a means of obtaining the large amplitudes that were of interest. Next, to verify the results, a second methodology was employed using shaker testing. It was found that both the stiffness and hysteretic damping decrease with increasing displacement. However, they both approached asymptotes around 2 mils of displacement, and further increases in displacement had significantly less effect on the properties. Once the results were verified to be consistent, equations were obtained to describe the response of the wire mesh dampers. These equations were then used to create a new design workbook, which would allow an engineer to determine the properties of wire mesh dampers under conditions that they might experience.

ACKNOWLEDGEMENTS

First, I am thankful to Dr. Vance for not only allowing me the opportunity to conduct research at The Turbomachinery Laboratory and to complete my degree, but also for providing advice on the means of carrying out my research, and knowledge in the understanding of rotordynamics. Next, I am grateful for the unreserved assistance from my friends at the lab and the camaraderie they provided. They include, but are certainly not limited to: Ahmed Gamal, Mohsin Jafri, Aaron Schomerus, and Vinayaka Rajagopalan. Finally, I thank Drs. Malavé and Palazzolo for their time and effort in serving on the committee.

TABLE OF CONTENTS

Page

LIST OF FIGURES

LIST OF TABLES

CHAPTER I
INTRODUCTION

Motivation

Wire mesh dampers are under investigation because they are seen as replacements for squeeze film dampers as a source of direct stiffness and damping at bearing locations. There are several advantages of wire mesh dampers over squeeze film dampers. The wire mesh is relatively insensitive to operating temperatures between -310 and 217 °F. This extends their use into cryogenic machines, where squeeze film dampers cannot operate. The wire mesh is attractive in that it does not use oil to operate. For the inclusion in aircraft engines, their ability to sustain large amplitude vibrations without magnifying their effects, such as occur during blade-loss events, is also attractive. Also, wire mesh dampers would be favorable replacements for elastomer dampers in the vacuum environment of an energy storage flywheel, due to their ability to conduct heat away from the bearings. Furthermore, due to their direct damping, and lack of cross-coupled stiffness, the wire mesh reduces the response to imbalance and increases the stability of the system.

Need Statement

Several researchers at The Turbomachinery Laboratory have studied wire mesh dampers. However, most previous experiments were limited to zero-to-peak vibration amplitudes of less than 2 mils. Although most turbomachines operate within that range, it is possible that a turbomachine will experience larger amplitudes. Therefore, there is a need to determine the properties of the dampers under larger amplitude vibrations such as large imbalances or an impact from blade-loss.

Literature Review

A report by Childs [1] showed that wire mesh could provide equivalent stiffness and had good damping characteristics for the space shuttle's main engine high-pressure fuel turbopump. The dampers were also shown to have asymmetric stiffness, which has

---

This thesis follows the style of the ASME Journal of Engineering for Gas Turbines and Power.

a stabilizing effect in turbomachinery. Hara [2] demonstrated that an increase in the density of a mesh of steel wire increased its damping and stiffness. Burshid [3] tested a wire mesh damper and pocket damper seal hybrid to reduce leakage and counteract the negative stiffness of the pocket damper seal. He found that the mesh provided both stiffness and damping, and that their magnitude was increased with greater inlet pressures. Zarzour [4] replaced a squeeze-film damper with wire mesh in a rotating rig and showed that both the stiffness and damping of the wire mesh were advantageous in attenuating the response to imbalance. Zarzour and Vance [5] tested the wire mesh dampers while they were soaked in oil and demonstrated insignificant changes in the damping characteristics in the synchronous response, indicating that the damping is unlikely Coulombic in nature. With the same rig, the dampers were tested at temperatures up to 217 °F, and it was shown that the stiffness decreased slightly at elevated temperatures and the damping was unaffected. Al-Khateeb and Vance [6] found that the damping fits a hysteretic model better than a viscous model. Al-Khateeb [7] studied the effects of radial thickness, radial and axial interferences, amplitude, and frequency on the properties of the wire mesh. Ertas, Al-Khateeb, and Vance [8] showed that wire mesh could provide damping for liquid-fueled turbopumps by immersing dampers in liquid nitrogen and testing them at temperatures down to -310 °F. There were no significant changes in the damping of stainless steel meshes at cryogenic temperatures, whereas copper meshes showed increases in damping of around 25% over their ambient values. Choudhry [9] found that the stiffness and damping decreased as the axial and radial thicknesses of the wire mesh were increased. Choudhry and Vance [10] further developed a set of design equations to aid in the selection of wire mesh dampers for a turbomachine.

Objective

The research objective was to determine the properties of wire mesh dampers under large amplitude vibrations.

CHAPTER II
EXPERIMENTAL APPARATUS

Wire Mesh

One wire mesh element was used for this research, and is shown in Figure 1. It was in the shape of a hollow right cylinder and had an inner diameter of 3.99 inches, an outer diameter of 5.50 inches, and an axial thickness of 0.52 inches. The element was made from 0.0126-inch diameter copper wire knitted with a Jersey-Stitch pattern by the Metex Corporation. The element was knitted and then compressed into its final shape. This is the same material and stitch as the wire meshes that were used to formulate the previous design workbooks.

Figure 1. Wire mesh damper

Test Rig

A new non-rotating test rig was designed for these experiments. In the initial stages of impact testing, a previous rig -suitable for impact testing- was determined to be inadequate because both the wire mesh and the steel ring, in which it was housed, were never in the same locations after an impact hammer hit. The new rig was designed to

hold both the wire mesh and the ring in place at all times. The new rig also had an advantage over the cantilevered rig (another rig used previously): the angle between the centerlines of the inner and outer faces of the wire mesh is smaller at large amplitudes. This helped in maintaining equal displacement for the full axial thickness of the wire mesh damper. The test rig, shown in Figure 2, consisted of: a post, bolted to the foundation; a ring, which is supported by four threaded rods to prevent it from moving axially or angularly misaligning (which was a problem with the previous rig); and a cap, which was used to control the axial interference of the wire mesh. Figure 3 and Figure 4 show the side and top views.

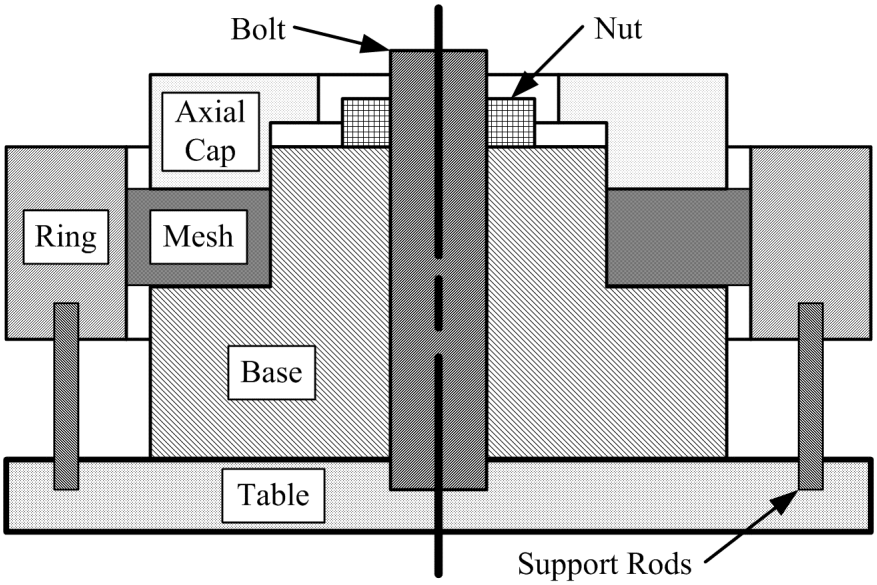

Figure 2. Section view of test rig

Figure 3. Side view of test rig

Figure 4. Top view of test rig with and without axial cap

Impact Instrumentation

For impact testing an ICP impact hammer approximately a meter in length was used. A Bently Nevada proximity probe faced the ring from the opposite end of the impact hammer and was attached to a magnetic base. This arrangement is shown in Figure 5. The impact hammer was mounted to a vertical metal arm that pivoted from a

supply pipe above the test rig, allowing the hammer to act as a pendulum. This led to increased repeatability of successive impacts, and aided in reducing data collection time.

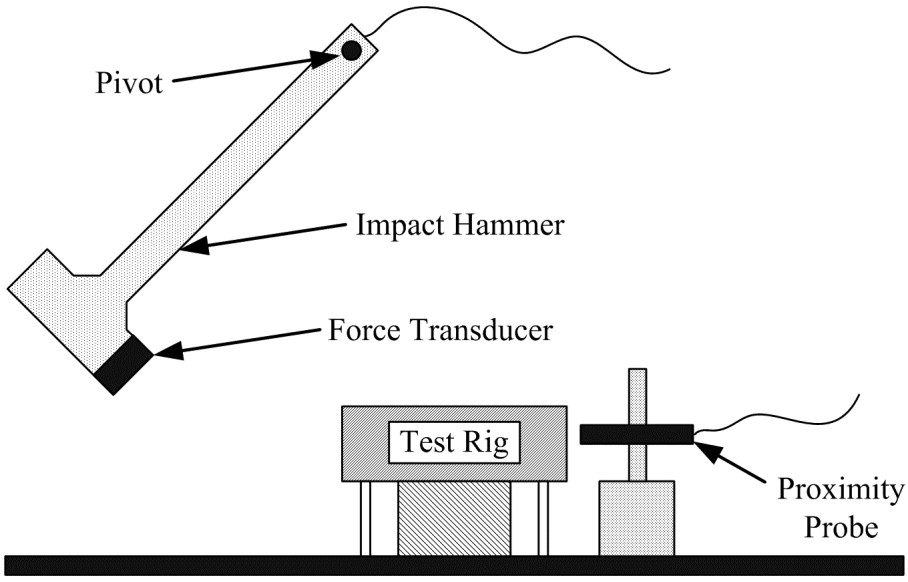

Figure 5. Diagram of impact instrumentation

Shaker Instrumentation

For shaker testing an MB Dynamics electrodynamic shaker was used. A simplified diagram of the test setup is shown in Figure 6.

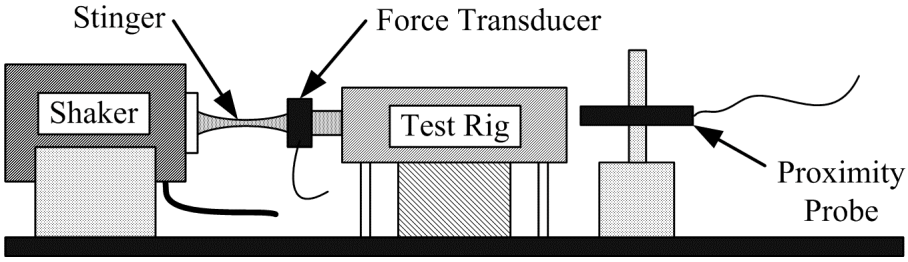

Figure 6. Diagram of shaker instrumentation

For clarity purposes, the proximity probe is shown arranged on the opposite side of the shaker. However, during testing the probe faced the same direction as the shaker. This arrangement is shown in Figure 7. The stinger consisted of a short threaded rod, and a longer flexible rod. A force transducer, used to measure the force transmitted into

the system, was between the two parts. The shorter part of the stinger was directly attached to the ring, so that that the force transducer correctly measured the force transmitted. Whereas errors can be introduced if the longer, flexible rod is in between the system and the transducer.

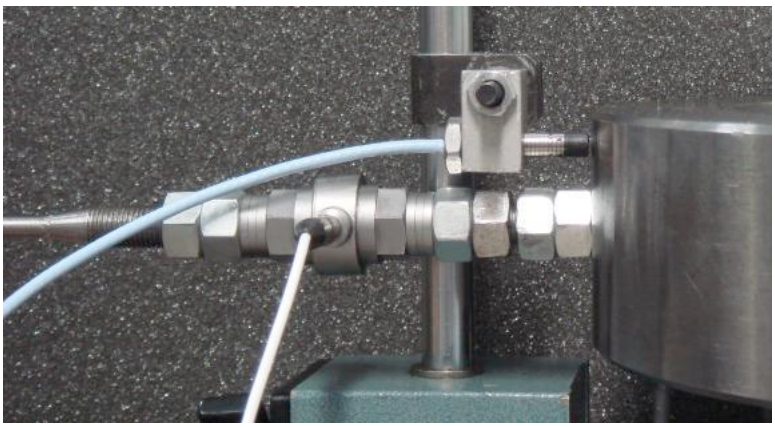

Figure 7. Probe arrangement for shaker testing

For the shaker testing, a PCI-6230 National Instruments Data Acquisition Board (DAQ) and a LabVIEW Virtual Instrument (VI) were used to take the data. LabVIEW provided the ability to quickly adjust the amplitude and frequency of the shaker force to meet the specific targets for each test. The target frequency and displacement amplitude were changed for each test by simple loops. Varying the force amplitude to achieve the target displacement amplitude was done through a feedback control specifically built to prevent damage to the instrumentation while being quick enough to minimize the degradation of the mesh and complete testing in a reasonable amount of time.

CHAPTER III
METHODOLOGY

Due to the difference in nature between the impact testing and shaker testing, two different data acquisition procedures were used. However, the parameter identification of the impact and shaker data was based on the same theoretical assumptions.

Data Acquisition

Impact Testing Procedure

When the impact testing was conducted, the displacement and force data were collected using a two-channel signal analyzer, the HP 35670A. The analyzer's trigger was tripped if the displacement went over 1 mil. This value was determined through trial and error as the lowest value that would consistently trigger the analyzer.

It was found from Sohaney [11] that when a zoomed frequency range is used, the built-in low-pass filter will delay some of the energy from the force transducer thus showing up in the time trace as ringing. To properly capture all of the energy Sohaney recommended the force window be 40 times the width of the impact duration. However, with the analyzer used, a force window would take an average of the time record outside of the window in order to make up a value for that time. Testing has shown that this leads to leakage errors in the frequency responses due to discontinuities between the value at the beginning and the end of the time block. Figure 8 demonstrates the error caused by using a force window on this analyzer.

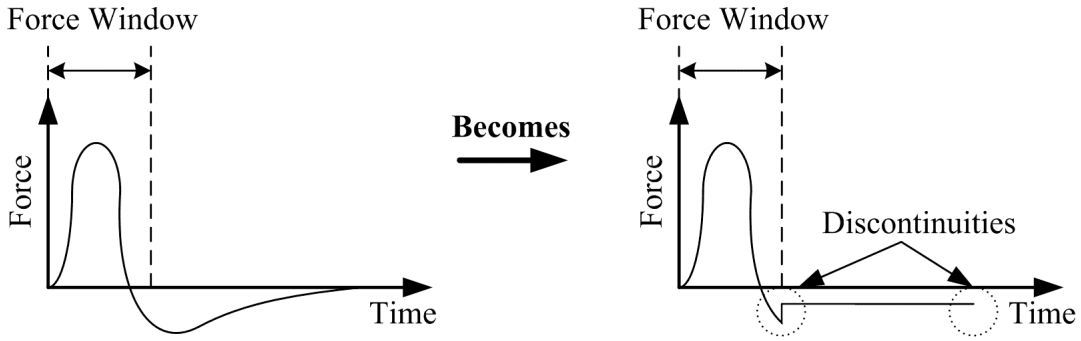

Figure 8. Example of discontinuities caused by force window

It was decided to use a flat top window, with a trigger delay of 0.5 seconds, to set the impulse right in the middle of the 1-second time block of 1,024 samples. An example of this is shown in Figure 9. This prevented leakage errors, correctly recorded the peak amplitude, and allowed the analyzer to capture all of the delayed energy of the pulse. For each impact, if the displacement was within 0.1 mils of the target value then it was manually accepted, and averaged, otherwise it was manually rejected. The analyzer averaged five acceptable impacts for each set of data at a specific displacement. To aid in analysis, the sensitivities of both the proximity probe and the force transducer were programmed into the analyzer so that all of the data transferred from the analyzer were in the units of interest.

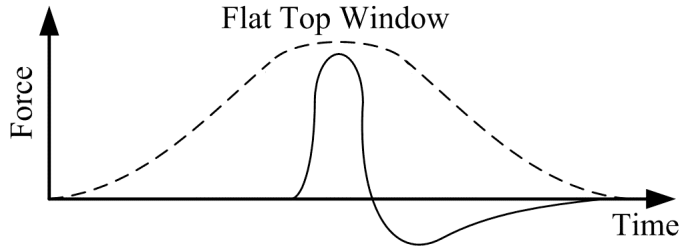

Figure 9. Example of flat top window with impulse

Before conducting any of the trials, the baseline modal parameters were determined, and then later checked for repeatability. Three groups of experiments were performed on the wire mesh element. The radial interference was first set to no interference. Next, for each value of axial interference, a set of displacement amplitudes

was tested. These steps were repeated for each value of radial interference that was tested. For each individual displacement set the analyzer recorded the real and imaginary parts of the transfer function from an average of five hits within 0.1 mils of the target displacement amplitude. Table 1 lists all of the values that were tested for each parameter during the impact testing.

Table 1. List of trials for impact testing

Parameter	Values Tested	Units
Radial Interference	0, 10.5, 20.5	mils
Axial Interference	0, 5... 25	mils
Displacement Amplitude	2, 4... 20	mils

Shaker Testing Procedure

When the shaker testing was conducted, both the displacement and force data were acquired and the shaker frequency and amplitude were controlled with a NI DAQ card and a LabVIEW VI that was created specifically for the task. Figure 10 shows the front screen of the VI that was created and used. The VI was designed to take all of the data with as little supervision as possible. It usually only required minor adjustments - from time to time- to the controller, in order to speed up the data collection. Since the shaker and force transducer had force limits of 100 lbs, there were data points that could not be taken. The controller would automatically switch to the next displacement set, or turn off the shaker, if the shaker reached its maximum force or the amplifier was unable to excite the shaker without clipping the waveform.

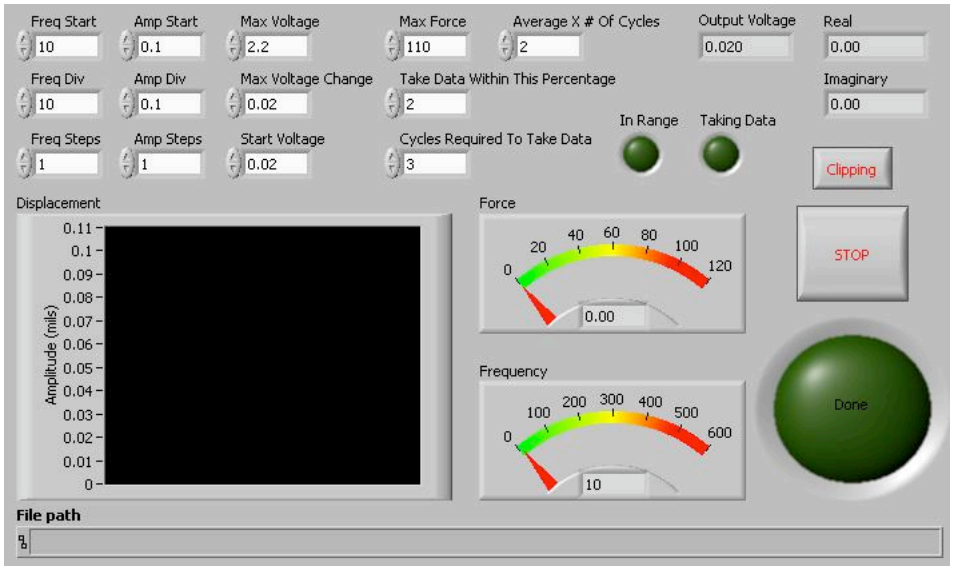

Figure 10. Virtual instrument for shaker tests

The following describes the data acquisition procedure that the VI carried out:

1. Generate a sine wave at the first frequency of interest (30 Hz was determined to be the lowest frequency that could be used without exciting the shaker's support structure). Then output this wave at 200,000 samples per second from the DAQ card to the amplifier.
2. Collect one time block of force and displacement data. This consists of one second at 2,000 samples per second.
3. Remove any DC bias, scale the voltages by the transducer sensitivities, and then perform FFTs on the force and displacement time data.
4. Use the complex FFT values at the current frequency and Equation 1 to obtain the zero to peak force and displacement amplitudes.

$$|x(f)| = \sqrt{\left(\text{real}(\text{x}(\text{f}))\right)^2 + \left(\text{imag}(\text{x}(\text{f}))\right)^2} \qquad (1)$$

5. If the displacement was not within 2% of the target displacement, adjust the amplifier amplitude until the displacement was within the limits.

6. Prepare to save the data if the displacement was within 2% of the target displacement for a continuous 3 seconds, it prepared to save the data.
7. Divide the complex FFT value of force by the complex FFT value of the displacement to obtain the complex value of the transfer function.
8. Save the real and imaginary values of the transfer function, as well as the current force, displacement, and frequency.
9. Increase the frequency by one step, and repeated steps 2 through 8.
10. Increase the amplitude by one step, and repeated steps 1 through 9.

After the VI completed each set, the axial interference and/or the radial interference were adjusted for the next set. Table 2 lists the values that were tested for each parameter during the shaker testing.

Table 2. List of trials for shaker testing

Parameter	Values Tested	Units
Radial Interference	0, 7.5, 10.5, 15	mils
Axial Interference	10, 15... 30, 40, 50	mils
Displacement Amplitude	0.1, 0.5, 1, 1.5, 2, 4... 20	mils

Parameter Identification

Impact Technique

In the frequency range of interest, the test rig was a single degree of freedom system. Equation 2 is the second-order non-homogenous linear differential equation with constant coefficients that is representative of the model. The forcing function and particular solution are assumed complex. The forcing function and particular solution are then substituted into Equation 2. After some algebraic manipulations, the transfer function, Equation 3, is obtained.

$$m\ddot{x}(t) + c\dot{x}(t) + kx(t) = f(t) \tag{2}$$

Where $x(t) = Xe^{i\omega t}$ and $f(t) = Fe^{i\omega t}$, which leads to:

$$F/X = \left(k - m\omega^2\right) + i(c\omega) \tag{3}$$

In the derivation of Equation 3, a harmonic forcing function was assumed. However, for the impact tests the forcing function was approximately an impulse. A perfect impulse would have had the effect of exciting all of the frequencies in the range of interest at the same amplitude. Notwithstanding, the impulse produced by the hammer occurs in a finite amount of time and therefore excited the higher frequencies with much less energy than the lower frequencies. Additionally, the curve of force versus frequency is almost parabolic in nature for low frequencies and at several points in the frequency domain it is nearly equal to zero. From Sohaney [11], an example of this is shown in Figure 11.

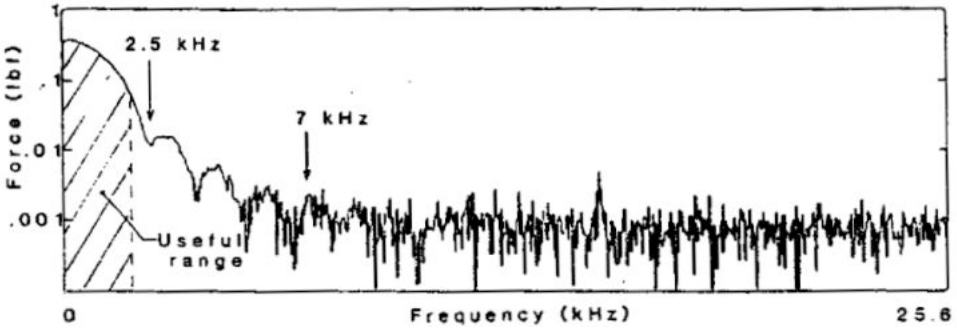

Figure 11. Example spectrum of force pulse

To extract the modal parameters from the transfer function, it is necessary to separate it into its real and imaginary components. Respectively, Equations 4 and 5 are the real and imaginary components of the transfer function.

$$\text{real}(F/X) = k - m\omega^2 \tag{4}$$

$$\text{imag}(F/X) = c\omega \tag{5}$$

The real part of the data is fitted to Equation 4, and the values for the stiffness and mass are calculated. From Equation 5, the damping value is determined from the slope of the imaginary part of the transfer function. However, experimentally it was

determined that the wire mesh does not behave as a viscous damper. Therefore, the damping was taken as the slope of an imaginary line drawn from the origin to the value of the imaginary part of the transfer function at $\omega=\omega_n$. This is shown in Figure 12 with an arbitrary curve as the imaginary part of the transfer function. The formula for this is shown in Equation 6. The natural frequency was calculated using Equation 7 when φ was 90°.

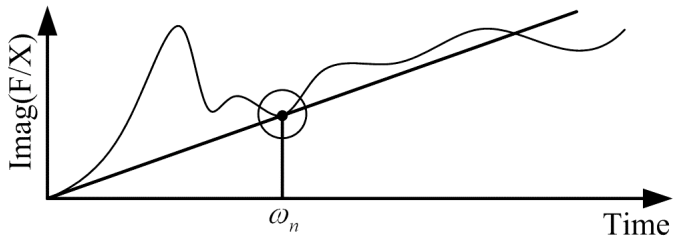

Figure 12. Example diagram of slope used to obtain damping

$$c = \frac{\text{imag}\left(F/X\right)_{\omega=\omega_n}}{\omega_n} \tag{6}$$

$$\phi = \tan^{-1}\left(\frac{c\omega}{k - m\omega^2}\right) \tag{7}$$

Shaker Technique

The parameter identification method used for the shaker data was similar to the method used for the impact data, with a few modifications. Since the shaker excited the system using a sinusoidal motion, Equations 2 and 3 were used without making any extra assumptions. However, because the system was only excited at one frequency at a time, a range of frequencies had to be tested to obtain enough data to complete the entire transfer function with respect to frequency.

It was decided to shake the system at only one frequency at a time to eliminate one major source of error. Due to the system nonlinearities with respect to displacement -which can be shown using linear techniques- chirp excitations produced erroneous results. This is because even though it is simple to maintain a constant peak voltage of a chirp excitation throughout a frequency range, the force required to achieve a target

displacement changes with frequency. This led to the displacement being different at every frequency swept by the chirp.

Using the mass and stiffness values for the baseline -which were obtained first and using the same method- the effect of the baseline was subtracted from the real part of the transfer function. This left only the stiffness of the wire mesh damper as a function of frequency, for a given amplitude.

When using the shaker data acquisition procedure, the baseline damping was found to be negligible and was not used to adjust the values taken from the wire mesh damper. When the imaginary part of the transfer function was studied, it appeared that the primary component of damping was hysteretic in nature, as the imaginary values did not seem to have any dependence on frequency. Therefore, the average of the imaginary values at a given displacement were taken as the hysteretic value for that displacement.

Methodological Differences

Stiffness Calculations

As seen in Figure 11, the spectrum of the impulse generated by the impact hammer was not constant. Instead, it tapered off as the frequency increased. Although the example spectrum was for force, the displacement spectrum would be similar. This leads to the conclusion that with impact testing, the displacement is a function of frequency, with the displacement values closer to 0 Hz being closer to the target displacement. Since the wire mesh's properties are nonlinear, different displacements will give different properties. In contrast, a linear system that would give the same modal values no matter the displacement. Therefore, the magnitude of the displacement at 0 Hz was approximately the target displacement. This leads to the conclusion that the ordinate intercept of the real part of the transfer function is approximately the stiffness of system for impulse testing. Under this conclusion, it can be assumed that given the same testing conditions, both the impact and shaker methods should calculate the same stiffness.

Damping Calculations

Unlike the stiffness, the equivalent viscous damping values that are obtained from the impact data are taken at a non-zero frequency -in practice the natural frequency. This is problematic because the displacement at that frequency is significantly below the target displacement. Therefore, due to the nonlinearities, the equivalent viscous damping values that are calculated using the impact data will not correspond to the damping values that would be obtained for the target displacement -had the impulse been perfect, and excited all of the frequencies with the same amplitude- and cannot be compared to the damping values calculated from the shaker data as they misrepresent the damping at their target displacements.

CHAPTER IV
RESULTS

Baseline

The baseline modal parameters were measured before impact and shaker testing began, and again in the middle of testing, to check for repeatability. Table 3 shows the baseline value measured during impact and shaker testing. The baseline values were subtracted from the data that was obtained when a wire mesh damper was installed, to only show the effect of the wire mesh.

Table 3. Baseline values as measured

Parameter	Method	Units	Mean
Weight	Average of Both	lb	15.0
Hysteretic Damping	Shaker	lb/in	0.12
Stiffness	Average of Both	lb/in	1298

Excitation Frequency

The excitation frequency measurements were only taken for the shaker testing, as the impact method cannot control the specific frequencies that are excited. The LabVIEW VI that was used for taking the shaker data was set to take a full frequency sweep before going to the next displacement amplitude. The VI started at the lowest frequency, 30 Hz, and increased the frequency in divisions of 10 Hz until either 400 Hz or the limits of the amplifier or shaker were reached.

Figure 13 shows a plot of the real part of the transfer function versus frequency. The data was taken with 7.5 mils radial interference and 20 mils axial interference. The individual lines are different displacements, starting at 0.1 mils, and going up to 2.0 mils. The curves follow the expected shape for a linear system.

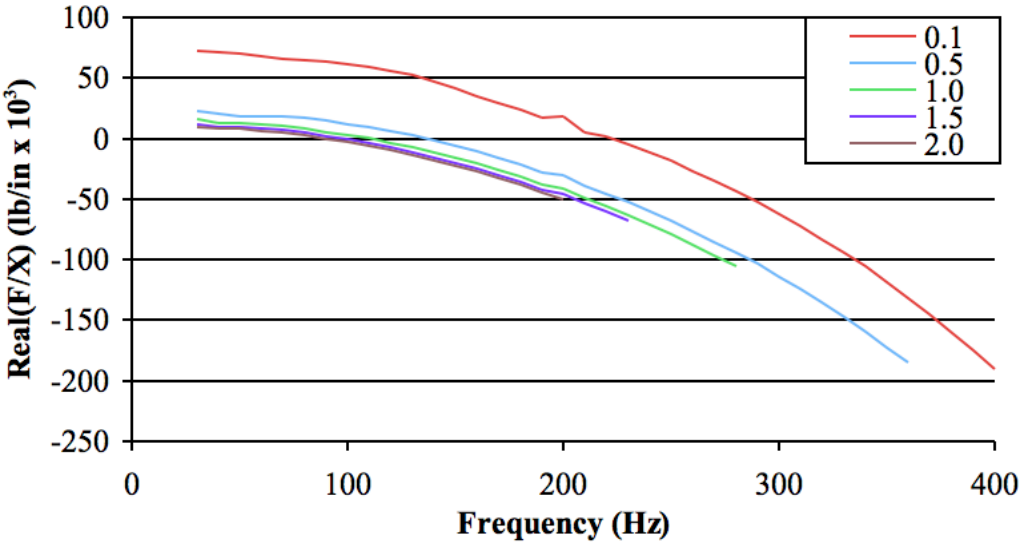

Figure 13. Real part of transfer function

The next step was to take the real values and subtract out the effect of the baseline. Equation 8 is the function that was used to obtain the stiffness as a function of frequency. Figure 14 is a plot of the stiffness of the same configurations that were plotted in Figure 13. The figure shows that for a given displacement, the stiffness remains relatively constant and appears to have no correlation with the frequency. Therefore, for every configuration tested, the stiffness value was taken as the average value from the frequency sweep.

$$k_{mesh}(\omega) = \text{real}(\omega) - \left(k_{base} - m_{base}\omega^2\right) \tag{8}$$

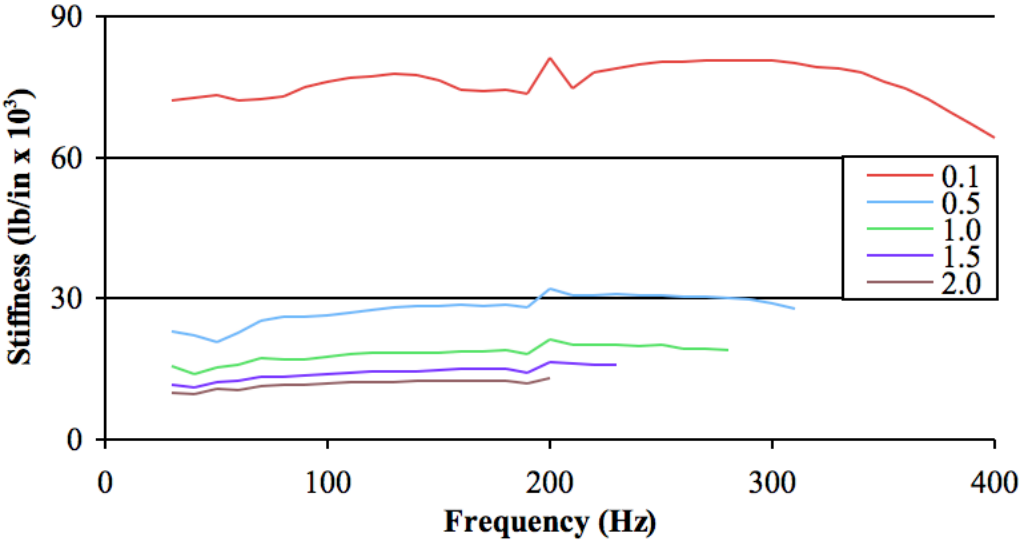

Figure 14. Stiffness as a function of frequency

The imaginary part of the transfer function is shown in Figure 15. This figure plots the same configurations that were shown in the two previous figures. Even though the data around the natural frequency of the proximity probe stand (200 Hz) is distorted, the values are relatively constant throughout the frequency range. This leads to the conclusion that the damping that is present in the wire mesh is primarily hysteretic in nature. Therefore, a hysteretic damping value was calculated for each configuration by taking the average value of the imaginary part of the transfer function throughout the frequency sweep (removing the points around 200 Hz, which were always distorted).

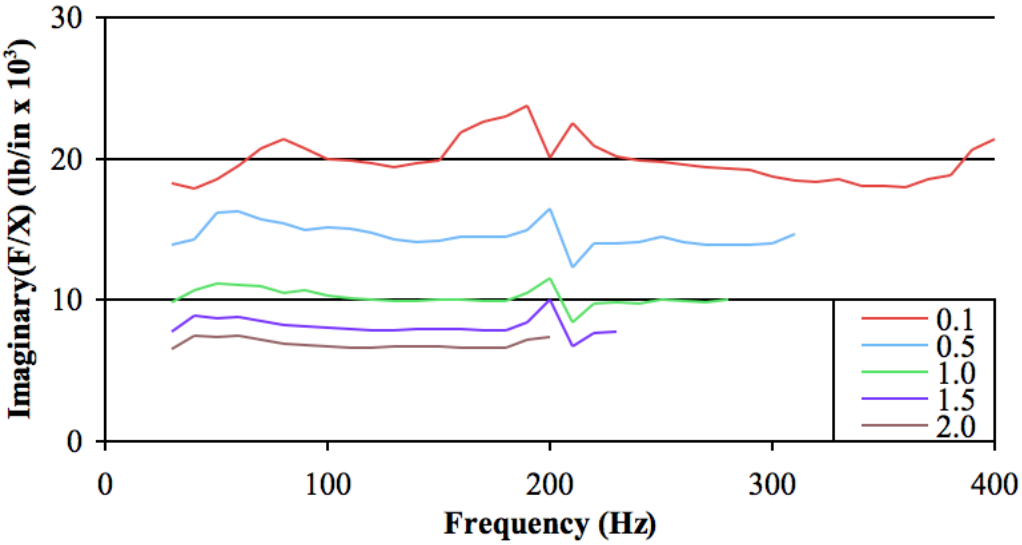

Figure 15. Imaginary part of transfer function

What is important to note about the shaker testing that was done for this research is that for all of the configurations that were tested the imaginary part of the transfer function was essentially a flat line -up to 400 Hz- for a given configuration. Previous investigations had used chirp or impact excitations, and as discussed in the methodology, these will not give the correct damping as a function of frequency for the wire mesh, and therefore parameter identification methods such as those that were employed for the impact testing had to be used to make sense of the data.

All of the example plots that are shown in the rest of this chapter have in common at least one point, the configuration with 10.5 mils radial interference, 20 mils axial interference, and 2 mils displacement. Although, for the specific variable that is being demonstrated, configurations of that variable above or below it are also shown. In each stiffness and damping figure there will be a fit line shown, this line is a representation of the formula that was calculated from all of the data. Its derivation and explanation are provided in the following chapter.

Displacement Amplitude

For impact testing, a full displacement set of 2 to 20 mils was recorded for each combination of radial and axial interference. The displacement amplitude was controlled by varying the angle from which the hammer was released. The data was accepted if the displacement amplitude fell within 0.1 mils of the target value. After each displacement amplitude was recorded, the analyzer's average was cleared and the next displacement amplitude was tested.

For shaker testing, a range of displacement amplitudes from 0.1 mils to 20 mils was taken for each combination of radial and axial interference -unless the limit of the amplifier or shaker was reached first. The VI would set the target displacement, and adjust the shaker amplitude until the displacement was within 2% of the target value.

Results

Figure 16 shows the stiffness as a function of displacement for both the impact and shaker testing under a configuration of 10.5 mils radial interference and 20 mils axial interference. The figure shows that the stiffness functions logarithmically decrease and are similar for both methods. This indicates that the data is consistent for the two methods employed.

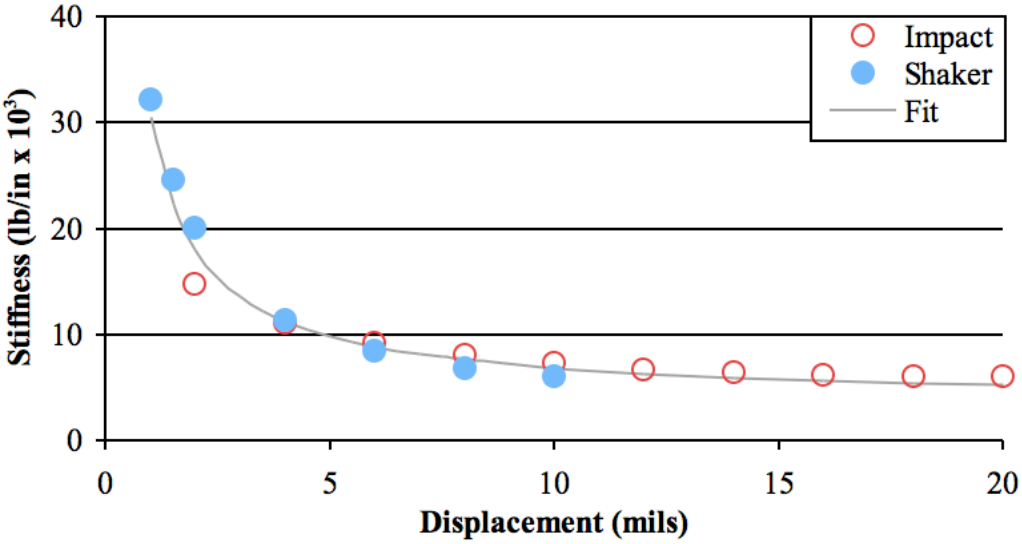

Figure 16. Stiffness as a function of displacement

Figure 17 shows the hysteretic damping as a function of displacement for the shaker testing. The hysteretic damping curve also decreases logarithmically as a function of displacement. Although Coulombic damping has been proposed as the source of damping in the wire mesh dampers, the fact that the damping is non-zero at low displacements -where the sliding necessary to produce friction would cease to happen- demonstrates that Coulombic damping provides a small or negligible contribution. To obtain the curve of equivalent viscous damping as a function of displacement, divide the values in Figure 17 by the frequency in rad/sec.

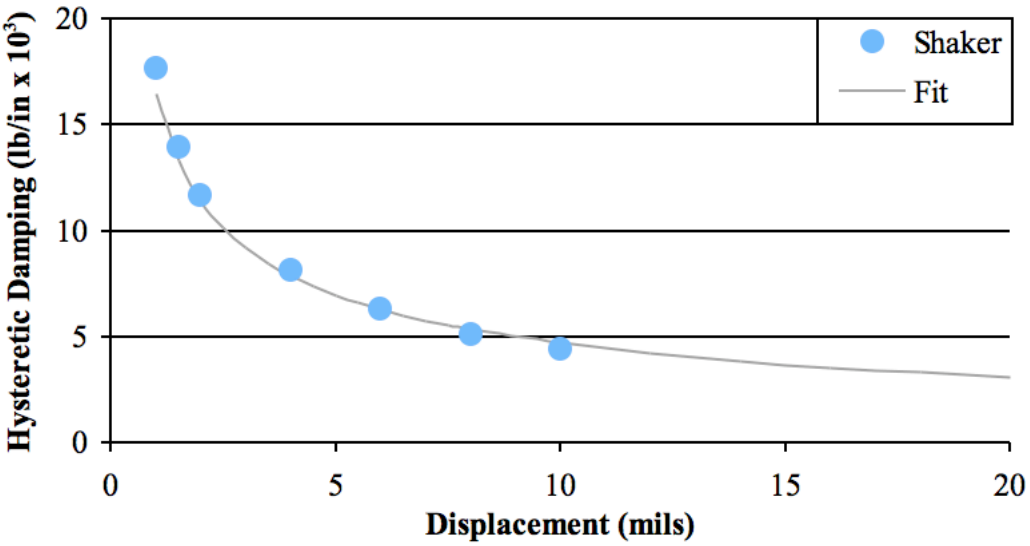

Figure 17. Hysteretic damping as a function of displacement

For both the stiffness and damping of the wire mesh, past researchers have also shown a decrease with increasing displacement. The current research used a fit that approximated the data that was obtained from both methods.

For hysteretic damping this is due to the structural bending, the loss factor should be constant. The loss factor is defined as damping divided by the stiffness. Figure 18 demonstrates the loss factor as a function of displacement using the parameters that were calculated for damping and stiffness. The curve is relatively flat for most of the range, and gives further evidence to support the damping being hysteretic in nature.

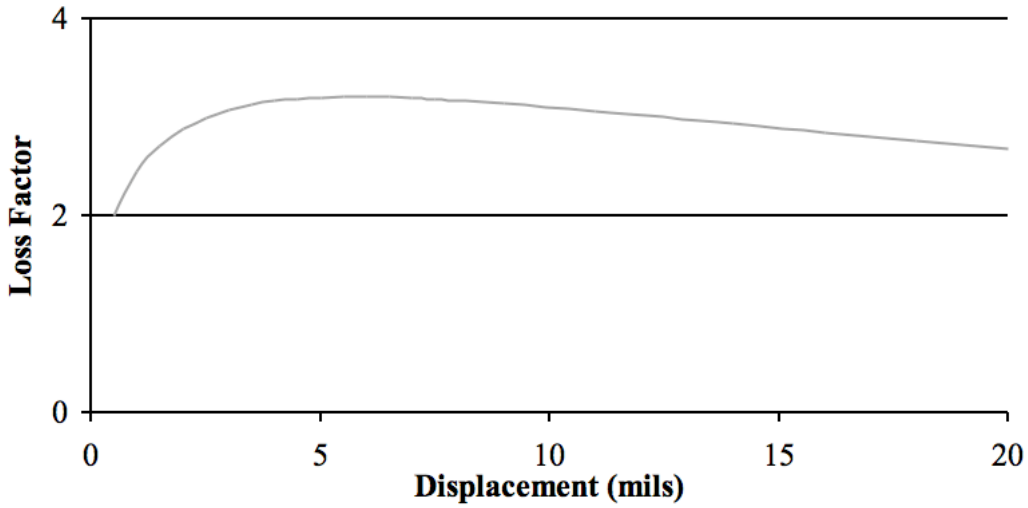

Figure 18. Loss factor as a function of displacement

Axial Interference

It was found early on that the functions for axial and radial interference found by previous researchers were not valid under the current circumstances, and so the effects of axial and radial interferences were tested along with the displacement amplitude for both impact and shaker testing. Zero axial interference was taken when the axial distance between the cap and base was equal to the average thickness of the wire mesh damper under no strain. This was done because under the application of radial interference, the wire mesh would deform and expand in the axial direction making a baseline measurement necessary. To increase the axial interference, the bolts holding the axial cap were tightened. The distance was checked with a caliper to ensure equal strain throughout.

When the data was taken for the shaker testing, axial interferences less than 10 mils were skipped, because it was found during the impact testing that under a combination of small axial and radial interferences the data was inconsistent.

Results

Figure 19 shows the stiffness as a function of axial interference for the impact and shaker testing under a configuration of 10.5 mils radial interference and 2 mils displacement. The figure shows that the trends both methods increase exponentially as a function of axial interference, and the values are similar in nature. This demonstrates that the data is consistent between the two methods employed.

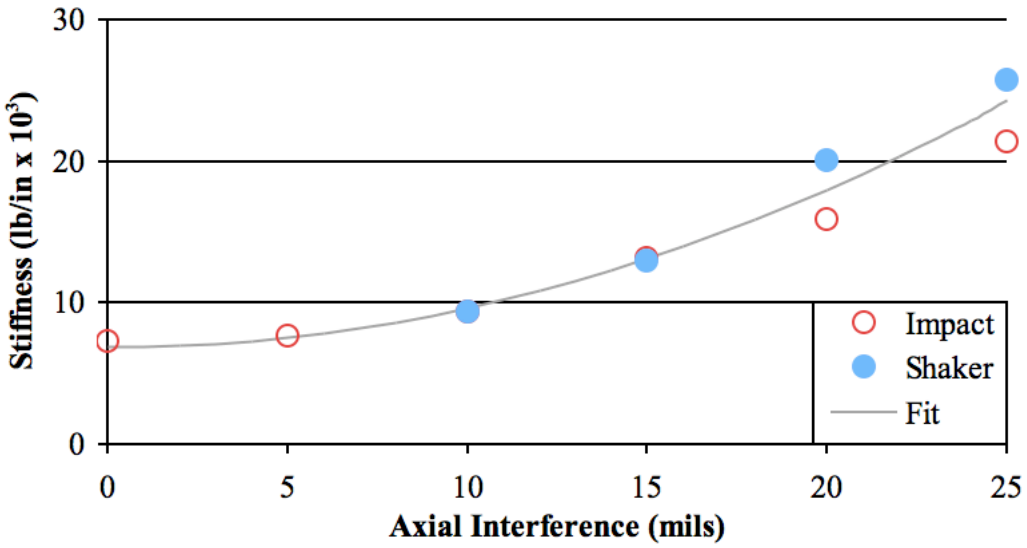

Figure 19. Stiffness as a function of axial interference

Figure 20 shows the hysteretic damping as a function of axial interference for the shaker testing. The data has a linear trend, and increases with increasing axial interference. To obtain the curve of equivalent viscous damping as a function of displacement, divide the values in Figure 20 by the frequency in rad/sec.

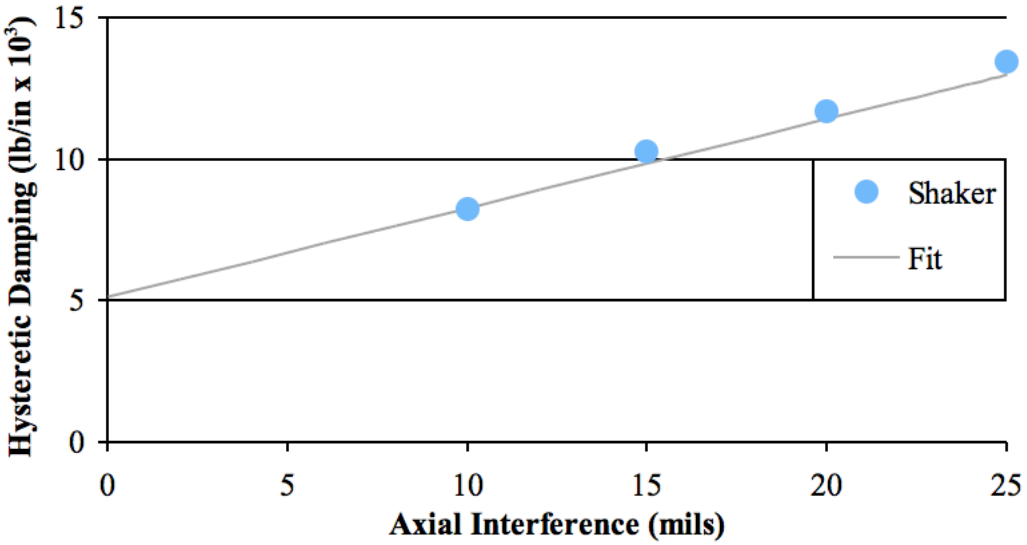

Figure 20. Hysteretic damping as a function of axial interference

Figure 21 demonstrates the loss factor as a function of axial interference. It demonstrates that the damping gradually decreases with increasing axial interference.

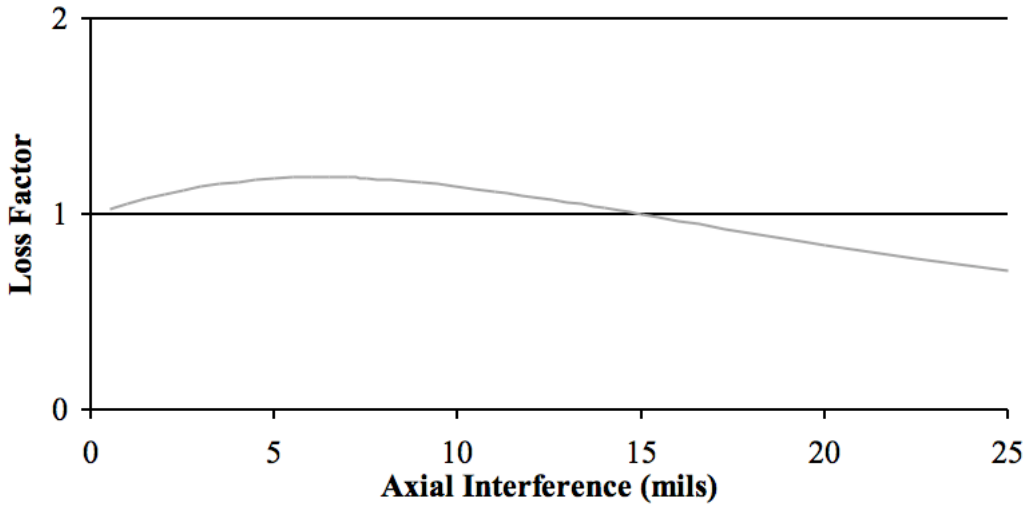

Figure 21. Loss factor as a function of axial interference

Radial Interference

The ring was originally machined to have zero radial interference with the wire mesh that was tested. To adjust the radial interference the inner diameter of the ring was changed with the addition of metal tape of specific thicknesses. This tape was assumed to have negligible affect on the data that was obtained.

Results

Figure 22 shows the stiffness as a function of radial interference for both the impact and shaker testing under a configuration of 20 mils axial interference and 2 mils displacement. The data has a linear trend, and increases with increasing radial interference.

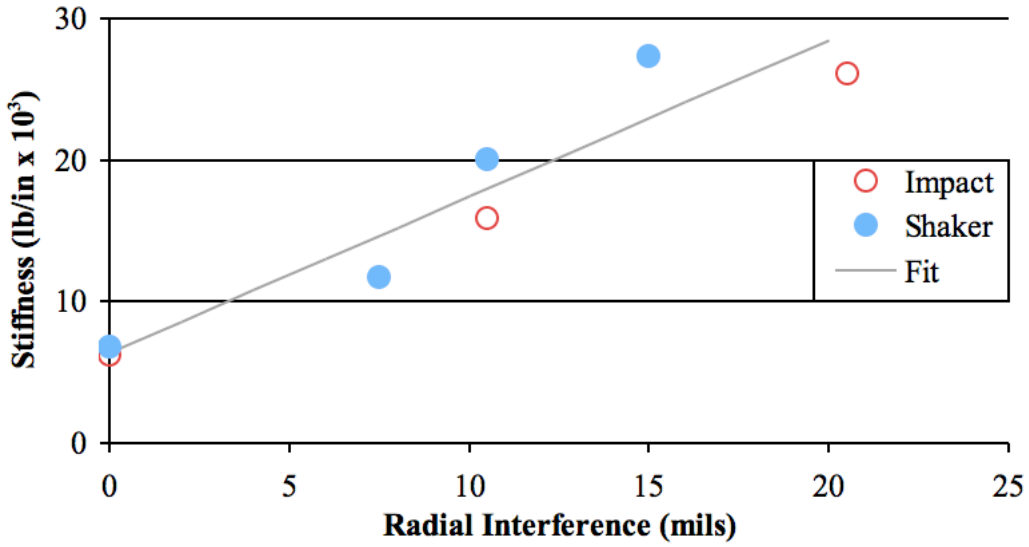

Figure 22. Stiffness as a function of radial interference

Figure 23 shows the hysteretic damping as a function of radial interference. The data has a linear trend, and increases with increasing radial interference. To obtain the curve of equivalent viscous damping as a function of displacement, divide the values in Figure 23 by the frequency in rad/sec.

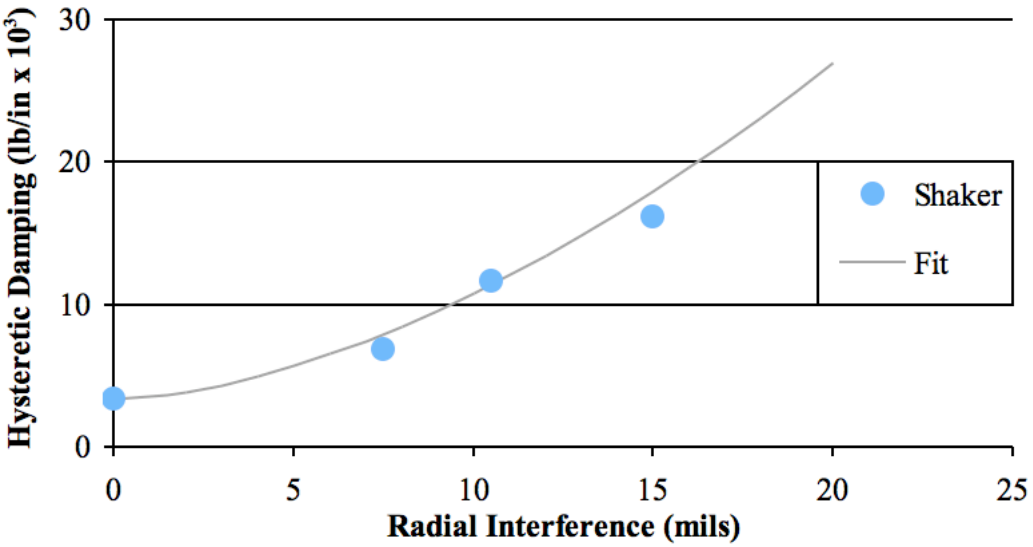

Figure 23. Hysteretic damping as a function of radial interference

Figure 24 demonstrates the loss factor as a function of radial interference. It demonstrates that the amount of damping increases as the radial interference is increased.

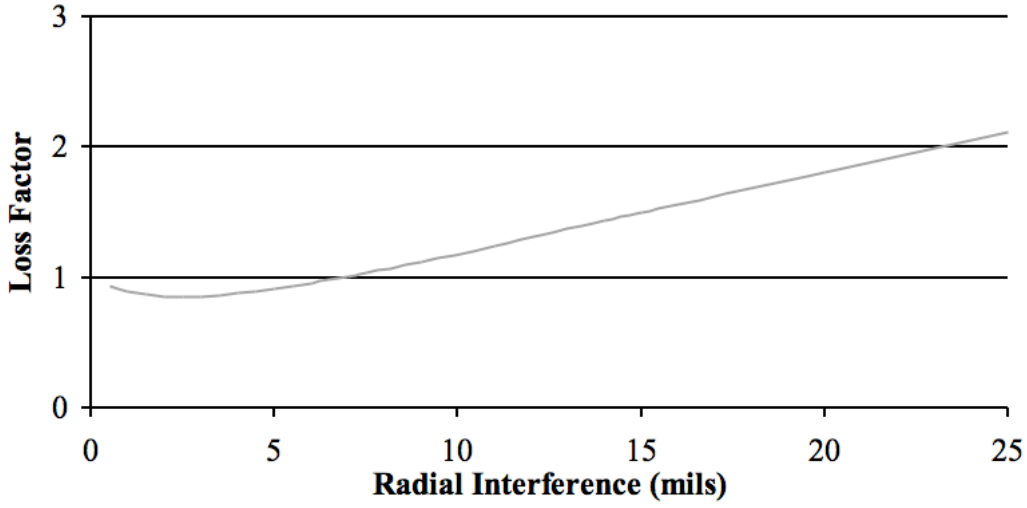

Figure 24. Loss factor as a function of radial interference

CHAPTER V
WIRE MESH DESIGN WORKBOOK

Modeling Wire Mesh Parameters

The effects that the displacement amplitude, axial interference, and radial interference had upon the modal properties of wire mesh were all studied. Since the ultimate goal was to provide a tool for predicting the properties of wire mesh dampers at any condition that a machine may encounter, cues from past research were taken into consideration. The equations formulated were to use dimensionless parameters and be in similar forms to past studies. The next step was to take the initial coefficients and equations, and use them to model all of the data that was taken. A solver was then used to adjust the coefficients, and reduce the error between the theoretical curves and the experimental data that was obtained. The adjustment of the coefficients was done so that the equations described all of the experimental data, not just the particular set that was used to obtain the coefficients of a particular factor. Table 4 shows each piece of the modal function as a function of a parameter that was found.

Table 4. Modal functions in terms of varying parameter

Parameter	Stiffness Function	Damping Function
Displacement	$8.06D^{-8/9}+1$	$23.2D^{-0.5}-1$
Axial Interference	$4.06e^{-3}A^{2}+1$	$6.09e^{-2}A+1$
Radial Interference	$1.71e^{-1}R+1$	$4.76e^{-2}R^{15/9}+1$

Each of the parameters were combined with the functions for the mesh geometry that were found by Choudhry [9]. The geometry functions for the radii and length of the wire mesh are shown in Table 5.

Table 5. Radius and length functions

Radii	Length
$\frac{R_o + R_i}{R_o - R_i}$	L

The parameters that were found were combined with Choudhry's functions to make the final equations. These were then multiplied by a constant that described the system. Equations 9 and 10 show the final equations. For the system that was tested, the K constant is 141 lb/in^2 and the H constant is 30.1 lb/in^2. However, the values for the constants K and H would likely be different for a different wire mesh. Experiments should be conducted on a sample mesh in one configuration to determine those values in order to use the equations to predict the properties of the wire mesh under other conditions. The values of displacement and interference are assumed to be in units of mils, and the values for the radii and axial length are assumed to be in units of inches - giving K and H in units of lb/in^2.

$$K = K_{const}\left(8.06D^{-8/9} + 1\right)\left(4.06e^{-3}A^2 + 1\right)\left(1.71e^{-1}R + 1\right)\left(\frac{R_o + R_i}{R_o - R_i}\right)L \tag{9}$$

$$H = H_{const}\left(23.2D^{-0.5} - 1\right)\left(6.09e^{-2}A + 1\right)\left(4.76e^{-2}R^{15/9} + 1\right)\left(\frac{R_o + R_i}{R_o - R_i}\right)L \tag{10}$$

Design Workbook

A workbook was created to model the experimental results that were obtained. The workbook uses the Equations 9 and 10 to allow one to determine parameters of similar wire meshes under investigation. The investigator should first use the "Factors" worksheet in order to determine the H and K constants that apply to the metal mesh in which they are interested. They would first enter the geometry of the mesh and then the constraints the system is under, in terms of axial and radial interference. Next, the investigator would have to excite the mesh in a rig similar in design to the rig used for these experiments -but with the necessary geometry for the intended application- with a

single sine wave at a chosen frequency and then enter the displacement amplitude and frequency at which the mesh was excited into the worksheet. It would probably be helpful to also excite the mesh under a few other amplitude and frequency combinations. The worksheet would then calculate the H and K constants for use in the "Design" worksheet.

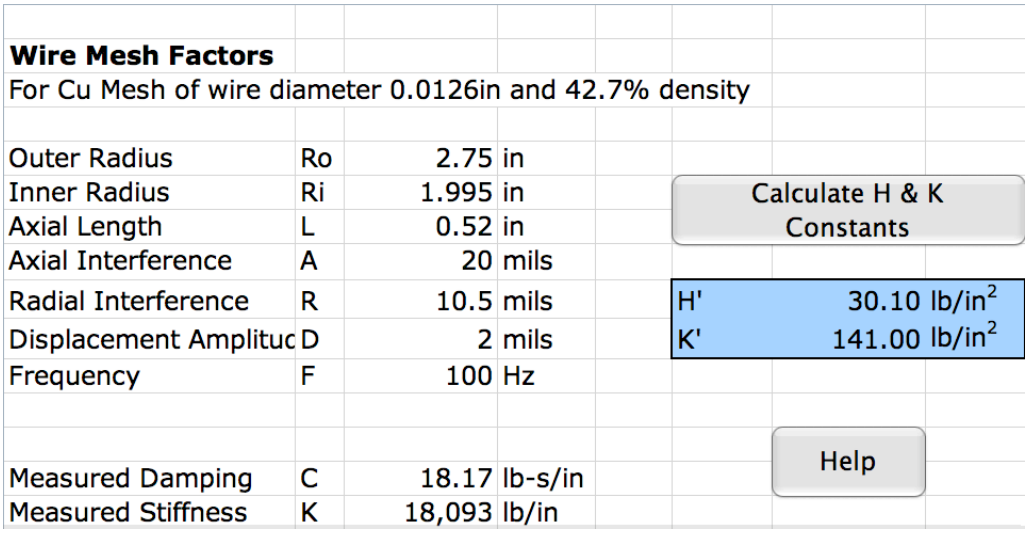

Figure 25. Wire mesh factor calculation worksheet

Once the investigators have the H and K constants for the wire mesh of interest, they can simply adjust the interferences, amplitude, and frequency to determine the stiffness and damping. For example, when looking at the measured damping and stiffness in Figure 25 the designers might see the mesh as inadequate, since they need the wire mesh to provide at least 28 lb-s/in damping at the running speed, 6,000 rpm (100 Hz). Since increasing the radial interference also increases the hysteretic damping, a quick solution would be to have a smaller radius in the support for the mesh to fit into - thereby increasing the radial interference. If the radial interference is changed to 20 mils, the equivalent viscous damping at the running speed is ~29 lb-s/in. The "Design" worksheet is where the designer would test these scenarios. The example that was just given is shown in the design sheet in Figure 26.

Wire Mesh Design

For Cu Mesh of wire diameter 0.0126in and 42.7% density

Outer Radius	Ro	2.75	in			
Inner Radius	Ri	1.995	in		Calculate K & C	
Axial Length	L	0.52	in			
Axial Interference	A	20	mils			
Radial Interference	R	15	mils	C	28.58	lb-s/in
Displacement Amplituc	D	2	mils	K	23,073	lb/in
Frequency	F	100	Hz			
					Help	
H constant	H'	30.10	lb/in^2			
K constant	K'	141.00	lb/in^2			

Figure 26. Wire mesh design worksheet

CHAPTER VI
CONCLUSIONS

Experimental Overview

The objective of this research was to determine the properties of wire mesh dampers under large amplitude vibrations. Impact testing was first conducted on the wire mesh as a means of obtaining the large amplitudes that were of interest with relative ease. In the course of investigation, it was decided to also take another look at how the radial and axial interferences affected the modal parameters. Next, to verify the results, a second methodology was employed -shaker testing- in order to eliminate any differences between current and past research experimental methods. It was found that both the stiffness and hysteretic damping decrease with increasing displacement. However, they both approached asymptotes around 2 mils of displacement, and further increases in displacement had significantly less effect on the properties. Once the results were verified to be consistent, equations were obtained to describe the response of the wire mesh dampers. These equations were then used to create a design workbook, which would allow an engineer to determine the properties of wire mesh dampers under conditions that they might experience. The equations could also be programmed into rotordynamic software to enable a designer to test how wire mesh dampers would perform and allowing the software to determine the properties iteratively.

Suggestions for Further Research

Although wire mesh dampers have been studied for several years at The Turbomachinery Laboratory, the understanding of the properties of wire mesh dampers is still severely limited. Before wire mesh is widely accepted as a replacement for squeeze film dampers, a more thorough understanding of the properties and limits of these dampers is necessary in order to fully exploit their potential and increase their attractiveness for use in new equipment. These are some of the tests that the researcher and some turbomachinery designers think should be conducted:

1. Greater variety of materials; only copper and stainless steel have been studied at The Turbomachinery Laboratory.
2. More wire weaves and geometries; all of the testing that went into design sheets used Metex's Jersey stitch, and only plain right cylinders have been tested -most with similar L/D ratios.
3. Greater densities; most of the dampers tested had a density of less than 46% (limited by the manufacturer, the Metex Corporation). Increasing the density was shown to increase stiffness and damping and testing should be done to determine the point at which the damping begins to be negatively affected.
4. Higher temperatures; such as those that would be experienced inside an aircraft turbojet or turbofan.
5. Another endurance test; to better control the shape of the mesh over time, to determine if the geometry or material has any affect on the endurance, and to determine if excitation frequencies have any affect on the endurance.

The most important of the research suggestions is number five. Before manufacturers will be willing to place wire mesh dampers in a machine where they are not easily accessible, or where downtime is an impossibility, they must have proven reliability and immutability. Where as the source of a squeeze film damper's properties -the oil- can simply be replaced to restore the damper's condition, it is not known for certain (at the moment) if there is such a corollary for wire mesh dampers, and the thought of extended downtime to restore or replace the damper should give designers pause.

Although there is still much testing that needs to be done on wire mesh dampers, they are a promising technology. Their ability to provide damping without oil -and even to do so in the presence of oil, without significant detriment- is a beneficial attribute. It is hoped that their advantages will inspire more research into their properties, and sway designers to use them in production turbomachines.

REFERENCES

[1] Childs, D. W., 1978, "The Space Shuttle Main Engine High-Pressure Fuel Turbo-pump Rotordynamic Instability Problem," Journal of Engineering for Power, **100**(1), pp. 48-57

[2] Hara, Fumio, 1992, "Characteristics of Steel Wire Mesh Friction Damping," ASME Pressure Vessels and Piping Division, **229**, pp. 155-161.

[3] Burshid, S. M., 1999, "Experimental Evaluation of Rotordynamic Coefficients for Hybrid Metal Mesh Pocket Damper Seals in Turbomachinery," Master's thesis, Texas A&M University, College Station, TX

[4] Zarzour, M. J., 1999, "Experimental Evaluation of a Metal Mesh Bearing Damper in a High Speed Test Rig," Master's thesis, Texas A&M University, College Station, TX.

[5] Zarzour, M., and Vance, J., 2000, "Experimental Evaluation of a Metal Mesh Bearing Damper," ASME Journal for Gas Turbines and Power, **112**(2), pp. 326-329.

[6] Al-Khateeb, E. M., and Vance J. M., 2001, "Experimental Evaluation of a Metal Mesh Bearing Damper in Parallel with a Structural Support," Proceedings of the ASME Turbo Expo 2001, New Orleans, Louisiana, June 4-7, no. 2001-GT-0247.

[7] Al-Khateeb, E. M., 2002, "Design, Modeling and Experimental Investigation of Wire Mesh Vibration Dampers," Ph.D. dissertation, Texas A&M University, College Station, TX.

[8] Ertas, B. H., Al-Khateeb, E., and Vance, J. M., 2003, "Rotordynamic Bearing Dampers for Cryogenic Rocket Engine Turbopumps," AIAA Journal of Propulsion and Power, **19**(4), pp. 674-682.

[9] Choudhry, V. V., 2004, "Experimental Evaluation of Wire Mesh for Design as a Bearing Damper," Master's thesis, Texas A&M University, College Station, TX.

[10] Choudhry, V. V., and Vance, J. M., 2005, "Design Equations for Wire Mesh Bearing Dampers in Turbomachinery," Proceedings of the ASME Turbo Expo 2005, Reno-Tahoe, Nevada, June 6-9, no. GT2005-68641.

[11] Sohaney, R. C., and Nieters, J. M., 1985, "Proper Use of Weighting Functions for Impact Testing," Proceedings of the International Modal Analysis Conference & Exhibit, 2, pp. 1102-1106.

APPENDIX A

Equipment

Device	Manufacturer	Model	Sensitivity	Units
Amplifier	MB Dynamics	SS530		
Analyzer	HP	35670A		
DAQ Card	NI	PCI-6230		
Force Transducer	PCB	222M08	47.11	mV/lb
Impact Hammer	PCB	086B50	0.85	mV/lb
Proximitor	Bently Nevada	3300		
Proximity Probe	Bently Nevada	3300, 5 mm	201.72	mV/mil
Shaker	MB Dynamics	PB-100A		

VITA

Adam Matthew Jones

9711 Walnut Woods Dr.
Kansas City, MO 64139

Education

Master of Science in Mechanical Engineering (Aug 2007)

Texas A&M University, College Station, TX

Bachelor of Science in Mechanical Engineering (May 2005)

Texas A&M University, College Station, TX

Experience

Rotordynamics Intern (Summer 2006)

Pratt & Whitney, East Hartford, CT